Renewable Energy 172 (2021) 382–391

Contents lists available at ScienceDirect

Renewable Energy

journal homepage: www.elsevier.com/locate/renene

Numerical analysis of the performance improvement of a flat-plate solar collector using conjugated porous blocks

K. Anirudh [a, b], S. Dhinakaran [b, *]

[a] Department of Mechanical Engineering, School of Technology, Pandit Deendayal Energy University, Raisan, Gandhinagar, 382 426, India
[b] The Centre for Fluid Dynamics, Department of Mechanical Engineering, Indian Institute of Technology Indore, Khandwa Road, Simrol, Indore, 453 552, India

ARTICLE INFO

Article history:
Received 22 October 2020
Received in revised form
21 February 2021
Accepted 23 February 2021
Available online 28 February 2021

Keywords:
Flat-plate solar collector
Conjugated porous blocks
Performance enhancement
Darcy-Brinkman-Forchheimer model

ABSTRACT

Performance enhancement of a flat-plate solar collector (FPSC) of direct absorption has been studied using porous insertions. The FPSC channel includes three conjugated porous blocks with various levels of permeability near the bottom insulator wall. Both the length and width of the blocks are altered near the inlet and outlet sections. The size of the middle trapezoidal block is aligned with reference to the gap available between the blocks near inlet and outlet. The parametric study focuses on finding the optimum design and arrangement of porous insertion. The height and width of the inlet sections are varied between 0 - H (step of 0.2) and 0-L (step of 0.2), respectively. The permeability of the porous blocks is varied between $Da = 10^{-3}$ - 10^{-1}. The opensource tool OpenFOAM® is used, and a generic steady-state thermal transport code is modified by the extended Darcy-Brinkman-Forchheimer model for realising porous medium. Numerical results indicate that the overall performance of the flat plate collector channel is improved by using the conjugated arrangement of porous bodies. The approach of placing the bodies near the bottom insulator plate improves heat transfer by promoting thermal mixing. Also, it is seen that more flow deviates towards the top absorber plate, and hence better thermal contact is established with the working fluid. The optimum performance is noticed for lower values of height of the block near the inlet and higher values near the outlet.

1. Introduction

The menaces posed by changing of climate has alerted the entire world. Its impact on human health and other environmental issues, as a result of a grave amount of fossil fuel burning, is well-known. Natural sources of energy, like solar and wind, are becoming popular and as immense research has been carried out for making their usage viable [1]. Amongst the various natural energy sources, solar energy is perceived as the cleanest and available readily in a useable form. Possibly because of this, the solar thermal systems have interested engineers and researchers for a long time.

The flat - plate solar collector (FPSC) is one amongst those many thermal systems, one of the oldest and simplest. However, due to its elementary design, it contains high heat losses and minor thermal efficiency. Various techniques have been in place to improve its thermal performance, as the insertion of porous materials. The porous medium is a popular passive method of improving heat transfer because of its tortuous paths and easy availability and installation. Specifically, when it comes to solar thermochemical reactors and thermal collectors, porous foams are a popular choice. The void filled structure promotes not only thermal mixing but also suppresses flow instabilities [2]. For instance, earlier numerical studies [3,4] have made it clear that inserting porous foam in FSPC, particularly near the top wall, results in a higher thermal gradient. As a result, lower thermal resistance is experienced by the movement of the working fluid. Furthermore, if the porous foam absorbs thermal energy from the incoming solar insolation, the fluid flowing through it obtains higher surface area of heat exchange. Hence, it would be interesting to look for chances to uplift design of the simple solar collector/heat exchanger design with the assistance of porous foam insertion [5].

Thermal characteristics of flow in a channel with porous insertions have been studied extensively. Chikh et al. [6] studied flow across porous blocks emplaced in a channel with the bottom heat source. Influence of the blocks' number and height is studied. The results indicated that the shear stress at the lower wall reduces due

* Corresponding author.
E-mail address: sdhina@iiti.ac.in (S. Dhinakaran).

https://doi.org/10.1016/j.renene.2021.02.145
0960-1481/

Nomenclature

$\bar{s}$	velocity of fluid in porous region, (m/s)
$\dot{Q}$	volume flow rate (lit/min)
C_p	specific heat at constant pressure $(J/kg \cdot K)$
D	diameter of the spherical particle of packed bed (m)
D_h	hydraulic diameter (m)
Da	Darcy number, κ/D_h^2
F	inertial factor, $(1.75/\sqrt{150}) \cdot (1/\varepsilon^{1.5})$
f_D	dimensionless pressure drop (friction factor)
H	collector channel height (m)
K	thermal conductivity of the material $W/(m \cdot K)$
k_{eff}	effective thermal conductivity, k_e/k_f
L	collector channel length (m)
Nu	local Nusselt number, $k_{eff}(\partial\theta)/(\partial Y)$
P	dimensionless pressure, $p/(U_\infty^2)$
P	kinematic pressure of the fluid, (m^2/s^2)
Pr	Prandtl number, ν/α
q_w	radiative heat flux (W/m^2)
Re	Reynolds number, $U_\infty \cdot D_h/\nu$
T	dimensional temperature, K
t	dimensional time, (s)
U, V	non - dimensional x, y - component of velocity, u/U_∞, v/V_∞
u, v	x, y - component of velocity (m/s)
X, Y	non-dimensional horizontal, verical distance, x/L, y/H
x, y	horizontal, vertical distance (m)

Greek

α	channel inclination angle $(\circ)$
Δ	largest grid size (m)
δ	smallest grid size (m)
ε	porosity
κ	permeability of the material (m^2)
ν	kinematic viscosity (m^2/s)
ρ	density (kg/m^3)
τ	non-dimensional time, $t \cdot U_\infty/D_h$
θ	non-dimensional temperature $(T - T_\infty)/(T_w - T_\infty)$

Subscript

∞	far field value
eff	effective value
empty	pertaining to empty channel
in	inlet value

to the presence of porous blocks. An augmentation in heat transfer is observed due to such occurrence. Guerroudj and Kahalerras [7] analysed mixed convection heat transfer in a channel with heated porous blocks of different shapes, placed over a local heat source. The presence of porous block improved the heat transfer immensely while causing an increase in the friction factor (f_D) value. The overall flow phenomenon remained indifferent to the presence of buoyant forces. In another study [8], they found positive inclination angles promote high heat transfer and lower pressure drop. Chen and Huang [9] performed numerical experiments from a strip heat source placed in a solar channel by discrete metal - foam blocks. These blocks are placed near the top wall of the channel, and it turned out to be a better choice of placement. Tuning porous blocks properties and adjusting the pressure drop resulted in higher thermal efficiency. In another study by Huang et al. [10] carried out with pulsating flow, similar outcomes are reported. Chen and Huang [9], Chen et al. [11] carried out a numerical study on the forced convection in a metal foam filled porous channel. The discrete heat source is placed on the bottom wall, and the channel is partially filled with porous foam. The results clarified that an undesired rise in pressure drop always accompanies the heat transfer enhancement because of porous insertion.

Numerous studies are available wherein porous substrates have been introduced in various forms for improving its thermal performance. Al-Nimr and Alkam [12] inserted porous substrates at the inner side of the collector absorber plate in a conventional tubeless collector. An augmentation in Nusselt number (Nu) up to 25 times is achieved by just filling the channel half with porous foam. However, a rise of up to 30 times in pressure drop is incurred in comparison to the empty channel. Further filling of the channel did not result in significant performance improvement. Alkam and Al-Nimr [13] reported similar outcomes for a tube-type solar collector, while the rise in Nu and pressure drop is reported up to 27 and 32 times. The optimum filling is found to be 0.8 times the characteristic height. Rashidi et al. [14] carried out a sensitivity analysis to check the effects of Da, Re, and porous substrate thickness on convection - radiation heat transfer in heat exchanged inserted with the porous medium. The results indicate pure dominance of Da over Re in affecting Nu and f_D values. Bovand et al. [15] further asserted that Nu rises with porous layer thickness at higher values of Da, while the reverse is true at lower Da values. Esmaeili et al. [16] carried out a numerical analysis to study the usage of metal oxide foams and water-based nanofluids as a solar absorber in a solar collector of direct absorption type. They expected the combination to have enhanced thermal performance in comparison to the empty collector. They concluded that the filled collector provided maximum enhancement in thermal performance. Numerical results implied that the collector efficiency using copper oxide nanofluid and metal oxide foam is enhanced by up to 26.8% and 23.8%, respectively. Yegane and Kasaeian [17] studied the thermal performance of a flat plate solar collector using a numerical approach. The collector channel is filled with porous media and is saturated with a hybrid nanofluid, and is subjected to a uniform magnetic field. A two-equation approach is also used to model the transport of heat transfer in the porous region. The increase in pore density resulted in a little increase in performance ratio for increasing porosity. It is seen that the overall performance of the collector rises at higher values of pore density, porosity, and Hartman number. Jouybari and Lundström [18] placed a thin porous layer near the covering absorber plate of a solar air heater and investigated its effect on thermal performance. Turbulent flow and heat transfer are simulated using a numerical approach. It is reported that the implementation of a thin porous layer results in a rise in thermo-hydraulic performance more than five times when compared with an empty channel. Moreover, such usage of a thin layer results in the reduction of the risk of hot spots and entrapped eddies are avoided. Conduction in the porous region is found dominant and influences the thermal and thermo-hydraulic performance of the solar air heater.

The above review clarifies on the increment of thermal performance in FPSC by using the porous medium. In an earlier attempt [3], multiple square porous blocks are placed near the top absorber plate of the FPSC channel, and immense rise in thermal

performance is reported. However, to the best of authors' knowledge, no numerical attempt has been made to investigate the influence of arrangement of rectangular and trapezoidal porous blocks near the bottom insulator plate for improving the design of a convectional FPSC of direct-absorption type. In the present parametric study, the influence of permeability and arrangement on the overall thermal performance is studied. Also, a comment is made on the usage of the inertial term in modelling the porous region. Authors sincerely believe that the present study shall provide an impetus for further physical and numerical experiments to explore the various porous insertion properties and configurations.

2. Mathematical formulation

2.1. Problem description

Numerical experiments have been performed for a laminar and an incompressible flow using the open-source finite volume method based tool OpenFOAM 5.0. Steady-state conditions have been assumed to prevail in the two - dimensional FPSC channel, which is inserted with porous conjugated blocks.

A schematic of the problem under consideration, along with boundary conditions, has been presented in Fig. 1. The working fluid is assumed to be water (Prandtl number, $Pr = 7$). The channel length and height ratio is set to around 60 so that the fully developed conditions are met sufficiently [19]. The upper layer of the channel is assumed to be a single layer comprised of glass, intermediate vacuum and absorber plate [14,15,19]. The porosity and permeability of the porous blocks is uniform, and it is saturated with a single-phase fluid (see Fig. 2).

The conjugated porous blocks are introduced in three different sections viz., inlet, middle, and outlet. The dimensions of the rectangular porous blocks near the inlet and the outlet have been varied. The middle trapezoidal block dimensions have not been explicitly varied, but are calculated to fill the gap uniformly. The filling is done such that the bottom face of this trapezoidal block matches with the insulator plate, while the top face is inclined and matches with the corners of the porous inlet and outlet sections, as shown in Fig. 1. The parameters related to the dimensions of the inlet and outlet porous blocks have been defined using the non-dimensional distances *SU*, *SD*, *DU*, and *DD*. The parameters *SU* and *SD* are calculated with respect to the collector channel length, while *DU* and *DD* with respect to the channel height. The distance

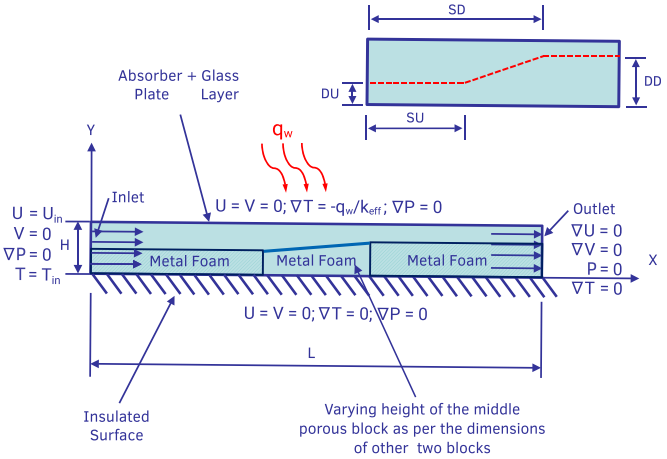

Fig. 1. Schematic of the computational setup detailing flow through the FPSC, along with boundary condition specifications, and details about the arrangement of the porous blocks is given.

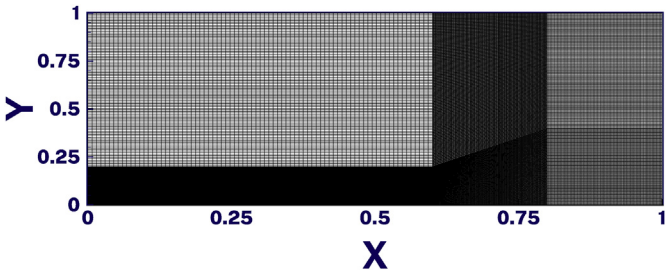

Fig. 2. Uniform structured distribution of mesh in the computational domain for simulating the steady incompressible fluid flow. The grid structure is plotted for $SU = 6L$, $SD = 0.8L$, $DU = 0.2H$, and $DD = 0.4H$.

SU is calculated from the inlet to front face of the middle block. The distance *SD* is calculated from the inlet to the front face of the outlet block. The distance *DU* depicts the height of the inlet block, while the distance *DD* represents the height of the outlet block.

It is assumed that the fluid enters the computational domain at uniform velocity (U_{in}) and uniform temperature (T_{in}). The Reynolds number of the flow is set to around 144 to correspond for a constant flow rate of 0.5 lit/min. A uniform heat flux (q_w) is applied at the upper absorber plate, representing the solar insolation. It is applied uniformly over the entire channel length and remains constant throughout the run. The local thermal equilibrium condition is assumed to prevail at the porous - fluid interface. Although this condition can be safely assumed for slow warming cases like the present study, a remark on this assumption is given.

2.2. Governing equations

Considering the assumptions as mentioned earlier, flow and heat transfer in the porous medium inside the channel can be modelled by.

Continuity Equation:

$$\frac{\partial u}{\partial x}+\frac{\partial v}{\partial y}=0, \tag{1}$$

Momentum Equations:

$$\rho\left(\frac{u}{\varepsilon^2}\frac{\partial u}{\partial x}+\frac{v}{\varepsilon^2}\frac{\partial u}{\partial y}\right)=-\frac{\partial p}{\partial x}+\frac{\mu_e}{\varepsilon}\left(\frac{\partial^2 u}{\partial x^2}+\frac{\partial^2 u}{\partial y^2}\right)-\frac{\mu}{\kappa}u-\frac{\rho F}{\sqrt{\kappa}}\left|\vec{V}\right|u, \tag{2}$$

$$\rho\left(\frac{v}{\varepsilon^2}\frac{\partial v}{\partial x}+\frac{v}{\varepsilon^2}\frac{\partial v}{\partial y}\right)=-\frac{\partial p}{\partial y}+\frac{\mu_e}{\varepsilon}\left(\frac{\partial^2 v}{\partial x^2}+\frac{\partial^2 v}{\partial y^2}\right)-\frac{\mu}{\kappa}v$$
$$-\frac{\rho F}{\sqrt{\kappa}}\left|\vec{V}\right|v, \quad \text{and,} \tag{3}$$

Energy Equation:

$$\left(\frac{u}{\varepsilon}\frac{\partial T}{\partial x}+\frac{v}{\varepsilon}\frac{\partial T}{\partial y}\right)=\alpha\left(\frac{\partial^2 T}{\partial x^2}+\frac{\partial^2 T}{\partial y^2}\right) \tag{4}$$

In the above equations, $\left|\vec{V}\right| = \sqrt{u^2+v^2}$ is the resultant velocity and $F = \frac{1.75}{\sqrt{150}}\cdot\frac{1}{\varepsilon^{1.5}}$ is the inertial factor [20].

Applying non-dimensional variables in OpenFOAM 5.0 is quite cumbersome, and hence, non-dimensionalisation of the output variables is done post-simulation, by using the following characteristic scales

$$X=\frac{x}{L},\quad Y=\frac{y}{H},\quad P=\frac{p}{\rho U_{\infty}^{2}},\ U=\frac{u}{U_{\infty}},\quad V=\frac{v}{U_{\infty}}\ \text{and}\ \theta=\frac{T-T_{\infty}}{T_{w}-T_{m}}. \tag{5}$$

2.3. Boundary conditions

During the solution of the above governing equations, details of the boundary conditions applied are displayed in Fig. 1. At the inlet of the computationsl domain, a uniform horizontal flow is incident, at an ambient temperature as $U = U_{in}$, $V = 0$, $T = T_{in}$ and $\nabla P = 0$. At the outlet of the domain, the 'inletOutlet' boundary condition is used, which applies $(\partial U)/(\partial X) = 0$, $V = 0$, $\nabla T = 0$ and $P = 0$. The bottom wall is insulated to avoid heat losses and a 'no-slip' condition is applied using $U = V = 0$, $\nabla P = 0$ and $\nabla T = 0$. The top wall is exposed to a constant heat flux 'q_w' and is introduced through the 'fixedGradient' condition using $U = V = 0$, $\nabla P = 0$ and $\nabla T = -q_w/k_{eff}$. The 'no-slip' condition is applied here as well.

3. Numerical details

The numerical experiments are carried out using the open-source finite volume method based tool OpenFOAM 5.0 [21]. The generic 'simpleFoam' solver has been modified by applying the extended Darcy - Forchheimer - Brinkman model and inserting temperature field. The solver is robust in handling steady-state laminar flow problems. The time derivative, gradient, divergence, and Laplacian terms are handled using the 'steadyState', 'Gauss linear', 'bounded Gauss linearUpwind', and 'Gauss linear corrected', respectively. All these are second-order schemes and are sufficient to handle the current computational exercise. Furthermore, the PCG solver, along with DIC preconditioner, is used to manage the pressure term. The PBiCG solver, along with DILU preconditioner, is used during the evaluation of velocity and temperature terms. The generic correction for pressure term is considered to be inspired by Rhie - Chow correction [22]. The residual criteria for the numerical solution are set as 10^{-6} for all fields, while under - relaxation factors of 0.3, 0.7, and 0.98 are applied for pressure, velocity, and temperature fields, respectively.

4. Grid generation and code validation

A structured uniform mesh is employed in the computational domain, wherein the trapezoidal regions have been considered separately for avoiding stepped porous region. The independence of the grid is verified by carrying out a grid dependence test at various porous blocks' height values. For the sake of brevity, the extreme case is shown at $SU = 0.2L$, $SD = 0.8L$, $DU = 0.2H$, and $DD = 0.8H$, for $Da = 10^{-3}$ (the notations refer to inlet and outlet block length and height, respectively).

The grid needs to be sufficiently fine to capture the flow in the gap between the porous block and the channel outlet. Also, it has to capture the boundary layers near the top absorber plate. Hence, four different grid sizes are chosen and tested using the Grid Convergence Index (GCI), given by Roache [23], based on Richardson extrapolation. It involves a comparison of discrete solutions of two different grid spacings. Based on the extrapolation technique, an exact solution is also estimated, a relative difference in comparison to this value is given. Very often three grid refinements are considered as f_1, f_2, and f_3 for fine, medium, and coarse grid structures, respectively. GCI value for the medium grid, with respect to the fine grid, is defined as,

$$GCI^{12}(\%) = 100 \cdot F_S \cdot \left(\frac{\varphi}{r^c - 1}\right) \tag{6}$$

here, F_S = factor of safety (usually kept to be 1.25), r = refinement ratio (considered to be 2), $\varphi = (f_2 - f_1)/f_1$ and c = order of convergence. The order of convergence (c), is then written as,

$$c = \frac{ln\left(\frac{f_3 - f_2}{f_2 - f_1}\right)}{ln(r)} \tag{7}$$

A similar relation would persist for the coarser grid with respect to the medium grid, given by GCI^{23}. The four grid sizes selected are 100 × 50 (Grid A), 200 × 100 (Grid B), 400 × 200 (Grid C), and 800 × 400 (Grid D). A comparison between the obtained results for these grid values in terms of local Nusselt number, friction factor, and the maximum temperature and velocity values at the outlet of the channel is given in Table 1. It is clear that the maximum GCI value is 0.395%, and the maximum relative error E_{RE} (calculated with respect to the f_{RE}) is 0.369%, which is below 0.5% and can assure fair confidence of the present results.

The numerical recipe has been thoroughly tested against the computational results of Morosuk [24] for various porous layer thickness and *Da* values, and satisfactory comparison is achieved. Moreover, the current code also shows excellent relevance with the computational results of Mohamad [25]. The local *Nu* at the right corner fo the top wall of the porous filled channel is compared. Furthermore, the existing code is also checked against the experimental results provided by Saedodin et al. [19] at different flow rates, and satisfactory conviction is achieved. Details of the comparison are shown in Figs. 3–5, respectively.

5. Results and discussions

Extensive two-dimensional numerical computations are carried out for understanding the influence of porous blocks' number, arrangement, thickness, and *Da*, on the flow patterns and heat transfer performance of a solar flat plate collector filled with porous metal foam blocks. Following range of parameters is considered during simulations:

- Darcy number, $Da = 10^{-3}$, 10^{-2}, and 10^{-1}.
- The dimensions related to the trapezoidal blocks' placement can be clearly seen in Fig. 1. Accordingly, *SU*, *SD*, *DU*, and *DD* represent the width of the upstream block, width of the downstream block, height of the upstream block, and height of the downstream block. The values of each of these parameter range between $0.2H$ to $0.8H$ (for *DU* and *DD*) or $0.2L$–$0.8L$ (for *SU* and *SD*).
- The height and width of the centre trapezoidal block depends on the upstream and downstream blocks' dimensions and it has to fill the gap accordingly.

5.1. Isotherm contours

While the water flows in the FPSC channel, which is filled with blocks made of uniform porous material, the channel length is kept sufficiently long. Hence, long before the fluid flow reaches at the end of the collector, the flow is fully developed. The case does not change even when the porous blocks almost fill the channel. Isotherm contours for the trapezoidal arrangement of blocks are shown in Figs. 6 and 7. In a previous attempt to enhance the performance of the FSPC channel using multiple identical porous blocks [3], the placement is near the top absorber plate. The school of thought in that study is to allow mixing of the fluid in the

Table 1
Grid dependence study details provided for $Da = 10^{-4}$ at a configuration with the dimensions $SU = 0.2L$, $SD = 0.8L$, $DU = 0.2H$, and $DD = 0.8H$.

Grid ($M \times N$)	E_{RE} (%)	Nu	GCI (%)	E_{RE} (%)	f_D	GCI (%)	E_{RE} (%)	θ_{max}	GCI (%)	E_{RE} (%)	U_{max}	GCI (%)
A (100×50)	3.239	33.128	0.683	4.713	3.619	1.110	1.300	1.560	0.607	0.643	4.073	0.037
B (200×100)	1.506	33.572	0.250	1.869	3.727	0.510	0.649	1.550	0.365	0.173	4.054	0.006
C (400×200)[a]	0.550	32.265	0.144	0.843	3.766	0.395	0.325	1.545	0.244	0.025	4.048	0.000
D (800×400)	0.201	32.153	–	0.369	3.784	–	0.130	1.542	–	0.000	4.047	–
f_{RE}	–	32.089	–	–	3.798	–	–	1.540	–	–	4.047	–

[a] Represents chosen grid for the study.

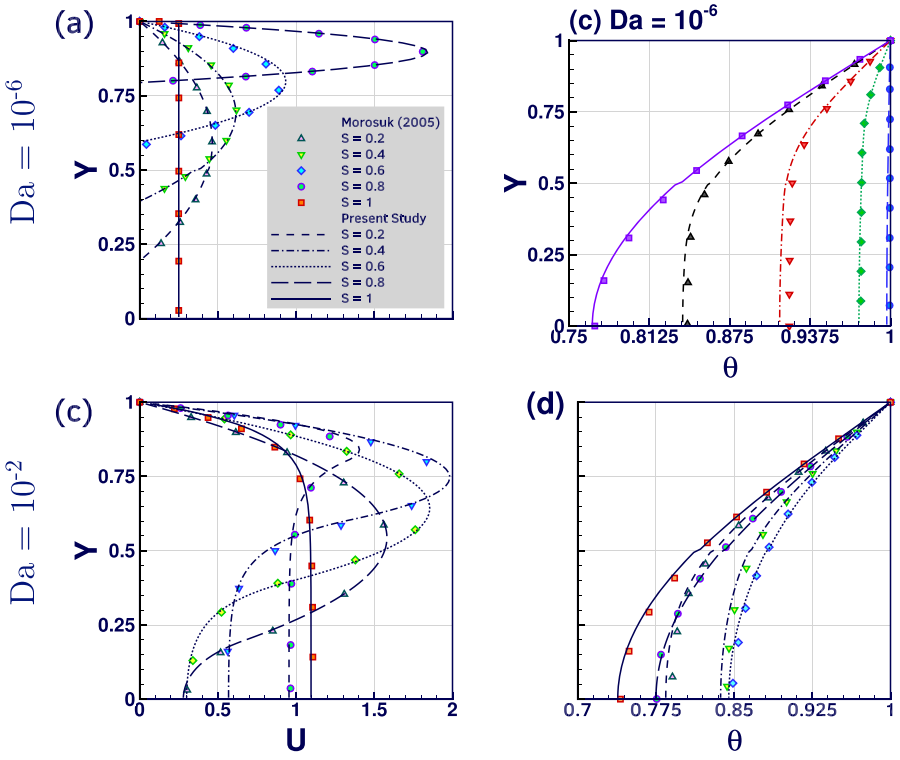

Fig. 3. Comparison of horizontal velocity (a, c) and temperature profiles (b, d) at the outlet of porous channel with Morosuk [24] at $Da = 10^{-6}$ (a, b) and 10^{-2} (c, d) for different porous block height (S) values.

thermal boundary layer region and allow storage of the heat captured from the solar insolation. In the present study, a contrasting thought is proposed, wherein three porous blocks of different shapes and sizes are placed near the insulator plate, allowing both mixing of the fluid and allowing free-flowing fluid to come in contact with the top absorber plate.

The height and width of the three blocks have been tampered for attaining optimum thermal performance. Dimensions of the porous blocks near the entrance and the exit of the collector channel have been changed. At the same time, the intermediate porous block takes the trapezoidal shape to fill the gap between the prior blocks. In the first case, shown in Fig. 6, the influence of permeability and exit block height of all the blocks has been tested. The variation in deviation of isotherms near the exit block upon increasing the ease of permeability is evident. As the Darcy number increases, more fluid enters the porous foam region, and cause better thermal mixing. Such a phenomenon affects the thermal boundary layer development, which changes with blocks' dimensions and porous properties. For instance, in the subplot (a), it is clear that the higher *DD* and lesser permeability causes a decline in the outlet temperature value, which is supported by the lower thermal contour value.

However, the development length of isotherm increases with permeability for the same height due to ease of flow through the narrow outlet region shown in subplot (b). Due to the reduction in *DD* parameter and restriction to fluid flow, the thermal contours appear to be uniformly spreading from the top absorber plate, and the presence of porous blocks is hardly visualised in subplots (c) and (d). Moreover, the lower inlet block height and the gradual surface offered the trapezoidal intermediate block provides a smooth transition to the incoming steady flow. Such a configuration favours better thermal mixing and promotes the formation of a thin boundary layer as more fluid is pushed towards the heated absorber plate. More amount of fluid absorbs heat from the heated absorber plate, and the close underneath porous blocks offers better thermal mixing. On the contrary, a reduction in the development length is apparent on mirroring the setup from Fig. 7. Here, the influence of the height of the porous inlet block is studied, keeping the size of exit block and its permeability value constant. The height inlet block size is creating a negative drop of pressure, causing a bottleneck effect and resulting in a thicker thermal boundary layer. A rise in the length of the inlet block seems to worsen this state through subplots (b) and (d).

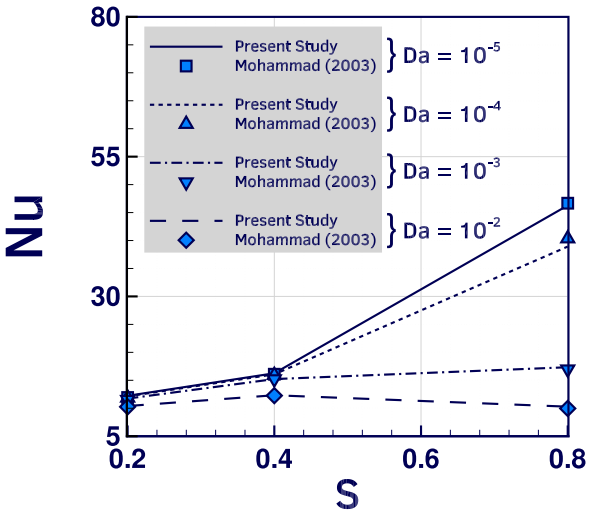

Fig. 4. Comparison of local Nusselt number (*Nu*) calculated at the top right corner of the porous channel with Mohamad [25] at various Darcy number (*Da*) and porous block height (*S*) values.

5.2. Local Nusselt number variation

After a numerical solution is reached, heat transfer at the top-right corner of the FPSC channel outlet is evaluated through the local Nusselt number. Variation in local *Nu* at different parameters considered in the study is consolidated through Fig. 8. The calculation behind the local Nusselt number stems from the combined numerical and experimental study carried out by Saedodin et al. [19], and it has been given below.

$$Nu = \frac{D_h}{T_w - T_m(x)} \left(\frac{\partial T}{\partial y}\right)_{y=H}. \tag{8}$$

In the above equation, $T_m(x)$ is the fluid bulk temperature and it is obtained as follows:

$$T_m(x) = \frac{\int_{y=0}^{y=H} uTdy}{\int_{y=0}^{y=H} udy} \tag{9}$$

The local *Nu* patterns for different values of *DD* have been given for two separate cases of *SU*, *SD*, and *DU*. The instances exhibiting

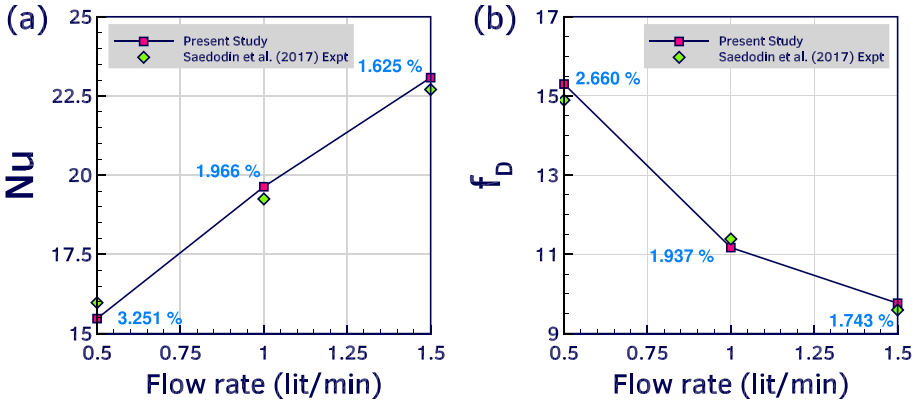

Fig. 5. Comparison of local Nusselt number at the top-right corner of FPSC outlet and friction factor across the domain with the experimental results of Saedodin et al. [19] at various flow rate values.

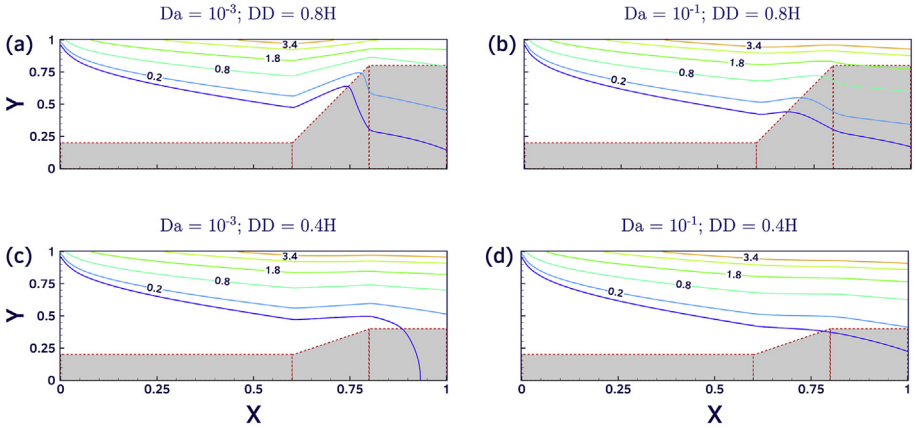

Fig. 6. Isotherm contours for $Da = 10^{-3}$ (a, c) and 10^{-1} (b, d) at $DD = 0.8H$ (a, b) and $0.4H$ (c, d), and $SU = 0.6L$, $SD = 0.8L$, and $DU = 0.2H$ blocks' height values.

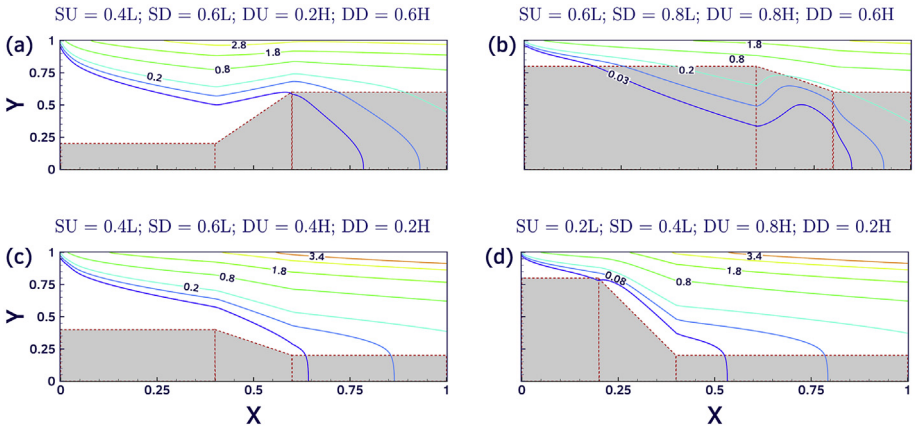

Fig. 7. Isotherm contours for various values of *SU*, *SD*, *DU* and *DD* at $Da = 10^{-3}$. For subplot (a), results for $SU = 0.4L$, $SD = 0.6L$, $DU = 0.2H$, and $DD = 0.6H$ shown. For subplot (b), results are $SU = 0.6L$, $SD = 0.8L$, $DU = 0.8H$, and $DD = 0.6H$ shown. For subplot (c), results are $SU = 0.4L$, $SD = 0.6L$, $DU = 0.4H$, and $DD = 0.2H$ shown. For subplot (d), results are $SU = 0.2L$, $SD = 0.4L$, $DU = 0.8H$, and $DD = 0.2H$ shown.

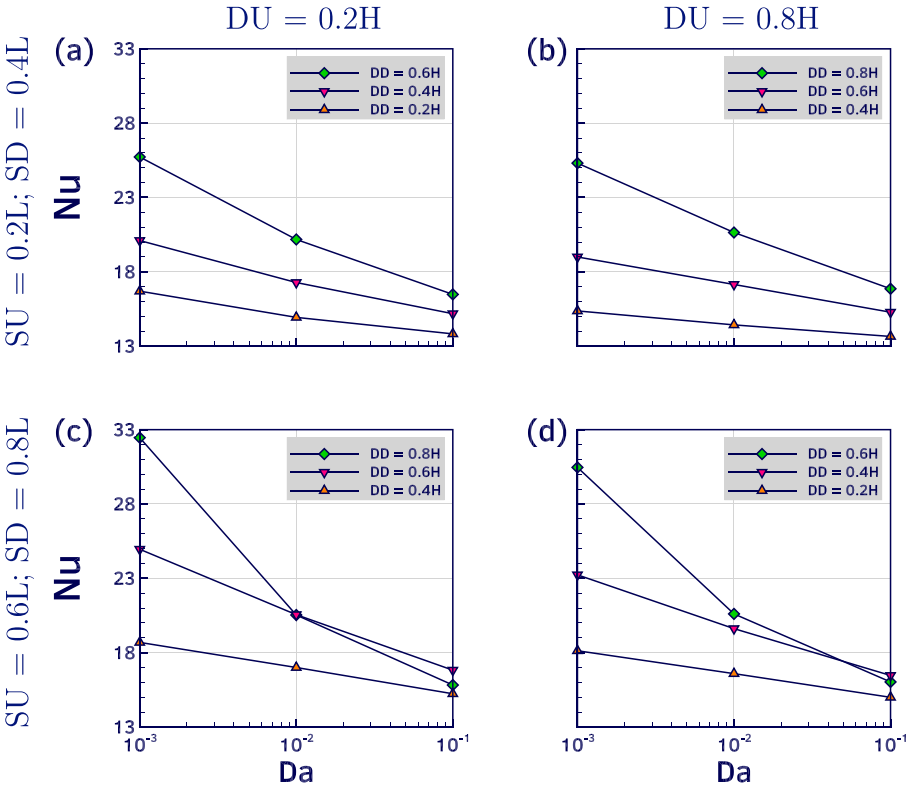

Fig. 8. Local Nusselt number variation at the top right corner of the channel at various *DD* values. The results for heights $SU = 0.2L$, and $SD = 0.4L$ are shown in subplots (a) and (b) for $DU = 0.2H$ and $0.8H$, respectively. The results for heights $SU = 0.6L$, and $SD = 0.8L$ are shown in subplots (c) and (d) for $DU = 0.2H$ and $0.8H$, respectively.

higher values of Nusselt number have been displayed in coherence with the isotherm contours discussed earlier. The subplots (a) and (c) represent $DU = 0.2H$, while the subplots (b) and (d) represent $DU = 0.8H$. Further, the subplots (a) and (b) represent $SU = 0.2L$ and $SD = 0.4L$, while the subplots (c) and (d) represent $SU = 0.6L$ and $SD = 0.8L$. The downfall in the Nusselt number can be discerned from the observations made from the isotherm contours for various cases.

As the exit block height is reduced and the permeability of the porous block rises, the thermal boundary layer thickens toward the channel outlet. Such a phenomenon results in the decrement of local *Nu* values. The heat transfer rate is naturally higher when the blocks are of greater height towards the outlet, because of promotion of close contact of the top absorber plate with the working fluid. Following this premise, the maximum value of local $Nu = 33.303$ is reported at $SU = 0.2L$, $SD = 0.8L$, $DU = 0.6H$, and $DD = 0.8H$. A comparable point can be seen in the subplot (c) for $SU = 0.2L$, $SD = 0.4L$, $DU = 0.2H$, and $DD = 0.8H$ with the local Nusselt number value of $Nu = 32.460$. In comparison to the earlier attempt [3] with porous layer near the absorber plate (max local $Nu = 16.435$ at $Da = 10^{-3}$), better heat transfer is reported for the same value of non-dimensional permeability. The augmentation in heat transfer in comparison to the empty ($Nu = 6.217$) and filled channel ($Nu = 16.249$ at $Da = 10^{-3}$) is notable [4]. However,

because of both introduction of porous blocks and narrow outflow region due to larger heights of the bodies, extra pumping power may be required, and the details follow.

5.3. Friction factor variation

Introducing porous foam not only improves thermal mixing but also bring the need for extra pumping power due to augmented flow resistance. Hence, while the usage of porous foam may be preferred for better heat transfer, the overall channel performance has to be taken into consideration. In the present case, since the height of the porous blocks and its porous properties are being tampered, some instances may introduce an unfavourable rise in pressure drop across the FPSC channel. Therefore, it is highly essential to check unwanted pressure losses so that the available energy can be utilised to its fullest with little rise in pumping power needs. The friction factor has been calculated using $f_D = (H \times \Delta P)/(0.5\rho u^2 L)$ and its trends are given in Fig. 9. Similar to local *Nu*, monotonous drops are reported in the f_D variation as well. The configurations selected during the Nusselt number discussion have been retained, and friction factor values are shown for these cases only.

When the height of the porous blocks and their permeability levels are reduced, resistance to the flow is lesser. As a result, the necessity for extra pumping power reduces, and hence, f_D trends fall. On the other hand, when the height of the porous blocks is more, although improvement is seen in heat transfer for all values of permeability levels, a rise in f_D can not be ignored. The maximum value of $f_D = 8.117$ is reported at $SU = 0.2L$, $SD = 0.4L$, $DU = 0.6H$, and $DD = 0.8H$ for $Da = 10^{-3}$. A closer point to this case can be visualised in subplot (a) for $SU = 0.2L$, $SD = 0.4L$, $DU = 0.6H$, and $DD = 0.6H$ at $Da = 10^{-3}$ with a value of $f_D = 8.078$. It should be noted that this rise is significant compared to f_D values of other cases and far more than the empty ($f_D = 0.217$) and but much less than the filled channel ($f_D = 28.103$ at $Da = 10^{-3}$) [3]. Moreover, the present arrangement of porous blocks fairs well when compared with the earlier placement near the absorber plate as the friction factor value, in that case, is $f_D = 18.702$ at $Da = 10^{-3}$ [4]. Usually, flow around rectangular porous objects have displayed a jump in flow properties [20,26,27]. But even with the present combination of multiple porous objects, no such occurrence is seen, and the traits remain consistent.

5.4. Performance evaluation criteria (PEC)

Upon studying the variation in local Nusselt number at the channel outlet and the friction factor trends, the performance needs to be calculated to make an informed judgement about the optimum dimensions of the porous conjugated blocks. Accordingly, a Performance Evaluation Criterion (PEC) has been utilised [19], which is given by, $\text{PEC} = (Nu/Nu_{empty})/(f_D/f_{Dempty})^{1/3}$. Here, the performance is calculated with respect to the empty channel. In contrast to the trends displayed in Figs. 8 and 9, the variation in PEC is interesting, as a balance is played out between the heat transfer augmentation achieved and the pressure drop born. Details of the PEC traits are given in Fig. 10. It is observed that for higher entry blocks height case, PEC values increase with Darcy number, as ease of flow is improved, and the friction factor value drops without much loss in heat transfer augmentation.

Also, when the overall porous blocks height is less than 0.4*H*, then the permeability variation has no effect on PEC prediction, as seen in subplot (c). In the case of the lower height of porous entry and intermediate height of the porous middle blocks, the dimensions of exit height block govern the overall thermal

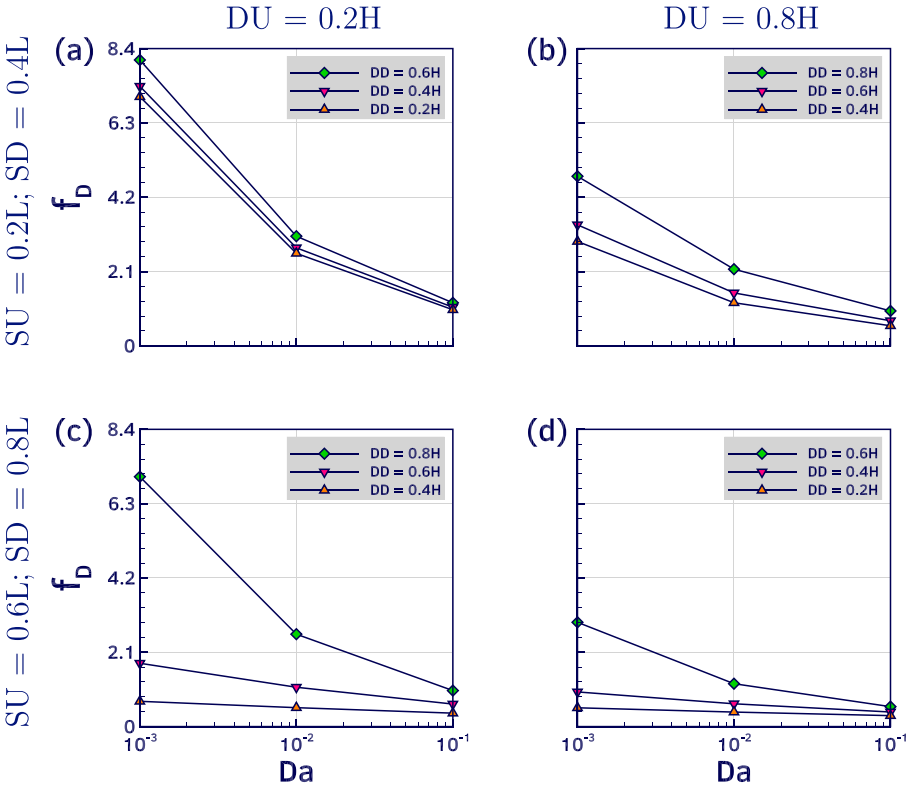

Fig. 9. Friction factor calculated across the channel at various *DD* values. The results for heights $SU = 0.2L$, and $SD = 0.4L$ are shown in subplots (a) and (b) for $DU = 0.2H$ and $0.8H$, respectively. The results for heights $SU = 0.6L$, and $SD = 0.8L$ are shown in subplots (c) and (d) for $DU = 0.2H$ and $0.8H$, respectively.

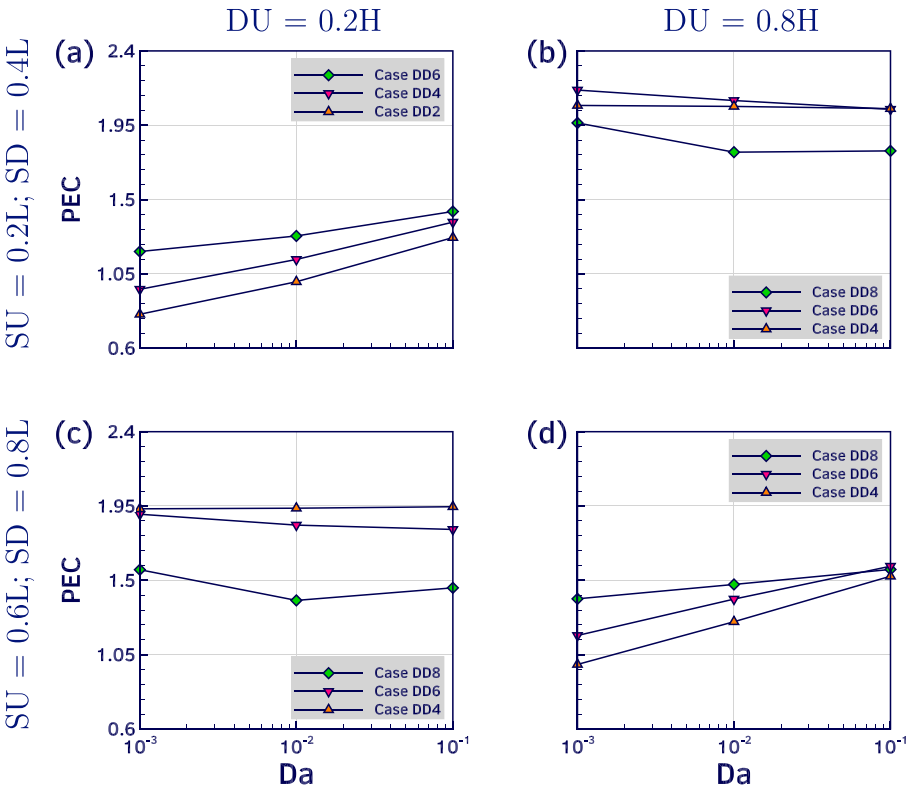

Fig. 10. Performance evaluation criteria calculated for the flat plate collector channel at various *DD* values. The results for heights $SU = 0.2L$, and $SD = 0.4L$ are shown in subplots (a) and (b) for $DU = 0.2H$ and $0.8H$, respectively. The results for heights $SU = 0.6L$, and $SD = 0.8L$ are shown in subplots (c) and (d) for $DU = 0.2H$ and $0.8H$, respectively.

performance. Higher performance is reported with a PEC value of 2.163 at $SU = 0.6L$, $SD = 0.8L$, $DU = 0.2H$, and $DD = 0.6\ H$, for the Darcy number value of $Da = 10^{-3}$.

While continuing the comparisons with previous arrangements, the present system fairs well, in terms of the overall thermal performance. Unlike previous sections, this relation is not limited to same permeability level, but from the perspective of the broad choice of parameters. It should be noted that since the flow rate and the dimensions of the FSPC channel are the same, the scrutiny holds. The maximum PEC value for the case of the porous filled channel is 1.614 (25.38% lesser than present PEC) at an inclination angle of 45°, Richardson number value of $Ri = 5$, the Radiation parameter value of $Rd = 5$ and $Da = 10^{-1}$. The higher thermal performance for the FSPC channel with porous insertion near the top absorber plate 1.959 (9.46% lesser than present PEC) with a long thin ($0.2H$) porous layer with the absence of porous medium at the inlet and the outlet. Based on this information, the present arrangement provides not only higher heat transfer augmentation and requires less pumping power, but also has higher performance than the earlier trials.

5.5. Darcy-Brinkman-Forchheimer extended model vs. Darcy-Brinkman model

In the present study, the extended Darcy-Brinkman-Forchheimer model is employed for realising the uniform porous medium. Since the flow rate is fixed, the inertial term from the model is scrutinised. The test has been carried out at several dimensional parameters considered in the study, and it has been observed that only Dary-Brinkman model is sufficient to model the current arrangement of conjugated porous blocks. Exclusion of the Forchheimer coefficient does not lead to erroneous values or divergence from the broad conclusion or the premise. For instance, at the optimum thermal performance case, the difference between the two models for calculating local Nu and f_D is 0.977% and 2.656%, respectively (the difference is calculated with respect to the extended model), and the maximum difference remains under 5%. A possible reason for this can be ascertained to the situation wherein significant flow occurs in the gap region between the absorber plate and the porous blocks and the permeable region mostly assists mixing. Because the current numerical exercise is the first of its kind, the computational results of the extended model are presented in this study.

6. Conclusions

Arrangement of conjugated porous blocks of various sizes and shapes in a direct absorption kind of flat plate solar collector (FPSC) has been numerically studied. Augmentation in heat transfer by making least compromises with excess pumping power demands has been focused. Computational experiments have been carried out by modifying a generic steady-state thermal transport code from the OpenFOAM® repository using the extended Darcy-Brinkman-Forchheimer (D-B-F) model with considerations of the superficial velocity. The primary parameters investigated are the permeability of the porous medium and the height and length of the two rectangular porous blocks. The size of the middle trapezoidal porous block is changed to adapt and fill the gap between the inlet and outlet blocks smoothly. Accordingly, four parameters are defined to ascertain the length and width of both the blocks. These parameters are *SU*, *SD*, *DU*, and *DD* that belong to the length and height of the inlet and outlet blocks, respectively. The dimension changes a step of $0.2H$ and $0.2L$, wherein H and L represent the height and length of the FSPC channel. The permeability of the

porous medium is varied in terms of a non - dimensional Darcy number as $Da = 10^{-3}$, 10^{-2} and 10^{-1}. The numerical results are presented in terms of non - dimensional isotherm contours, local Nusselt number (Nu), friction factor (f_D) and performance evaluation criteria (PEC). Because of the placement of the conjugated permeable bodies near the bottom insulator plate of the FPSC channel, not only thermal mixing of the fluid is promoted, but also more free-flowing fluid is encouraged to come in contact with the top absorber plate. Such a combination is seen to offer higher values of local Nu. Also, the friction factor values are found to be lesser in the cases where exit block height is larger than the porous entry block at all permeability values due to the bottle-neck effect causing adverse pressure gradient. It is inferred that lower height of inlet porous block, the intermediate transition of the middle trapezoidal block, and higher outlet porous block height result in comparatively lower f_D values. Upon evaluating the PEC criteria to identify an optimum setup, it is revealed that $SU = 0.6L$, $SD = 0.8L$, $DU = 0.2H$, and $DD = 0.6H$ offers the maximum PEC value of 2.163. A comparison with previous performance improvement trials has been made throughout the study for better insights. In terms of PEC estimate, the current approach provided higher values with an increment of 9.46% (evaluated with respect to PEC = 1.959 [4]) for the case of porous insertion near the top absorber plate. Also, a comment on the consideration of the inertial term in the extended D-B-F model is made. The results suggest that the exclusion of the Forchheimer term would not affect the outcome significantly. Experimental validation of the suggested arrangement can be carried out in the future along with the consideration of thermal buoyancy and its influence of the performance prediction.

References

[1] C.G. Granqvist, Transparent conductors as solar energy materials: a panoramic review, Sol. Energy Mater. Sol. Cell. 91 (17) (2007) 1529–1598.

[2] P. Vadász, Emerging Topics in Heat and Mass Transfer in Porous Media: from Bioengineering and Microelectronics to Nanotechnology, vol. 22, Springer Science & Business Media, 2008.

[3] K. Anirudh, S. Dhinakaran, Performance improvement of a flat-plate solar collector by inserting intermittent porous blocks, Renew. Energy 145 (2020a) 428–441.

[4] K. Anirudh, S. Dhinakaran, Numerical study on performance improvement of a flat-plate solar collector filled with porous foam, Renew. Energy 147 (2020b) 1704–1717.

[5] D. Poulikakos, M. Kazmierczak, Forced convection in a duct partially filled with a porous material, J. Heat Tran. 109 (3) (1987) 653–662.

[6] S. Chikh, A. Boumedien, K. Bouhadef, G. Lauriat, Analysis of fluid flow and heat transfer in a channel with intermittent heated porous blocks, Heat Mass Tran. 33 (5–6) (1998) 405–413.

[7] N. Guerroudj, H. Kahalerras, Mixed convection in a channel provided with heated porous blocks of various shapes, Energy Convers. Manag. 51 (3) (2010) 505–517.

[8] N. Guerroudj, H. Kahalerras, Mixed convection in an inclined channel with heated porous blocks, Int. J. Numer. Methods Heat Fluid Flow 22 (7) (2012) 839–861.

[9] C.-C. Chen, P.-C. Huang, Numerical study of heat transfer enhancement for a novel flat-plate solar water collector using metal-foam blocks, Int. J. Heat Mass Tran. 55 (23–24) (2012) 6734–6756.

[10] P.-C. Huang, C.-C. Chen, H.-Y. Hwang, Thermal enhancement in a flat-plate solar water collector by flow pulsation and metal-foam blocks, Int. J. Heat Mass Tran. 61 (2013) 696–720.

[11] C.-C. Chen, P.-C. Huang, H.-Y. Hwang, Enhanced forced convective cooling of heat sources by metal-foam porous layers, Int. J. Heat Mass Tran. 58 (1–2) (2013) 356–373.

[12] M. Al-Nimr, M. Alkam, A modified tubeless solar collector partially filled with porous substrate, Renew. Energy 13 (2) (1998) 165–173.

[13] M. Alkam, M. Al-Nimr, Solar collectors with tubes partially filled with porous substrates, J. Sol. Energy Eng. 121 (1) (1999) 20–24.

[14] S. Rashidi, M. Bovand, J. Esfahani, Heat transfer enhancement and pressure drop penalty in porous solar heat exchangers: a sensitivity analysis, Energy Convers. Manag. 103 (2015) 726–738.

[15] M. Bovand, S. Rashidi, J. Esfahani, Heat transfer enhancement and pressure drop penalty in porous solar heaters: numerical simulations, Sol. Energy 123 (2016) 145–159.

[16] M. Esmaeili, M. Karami, S. Delfani, Performance enhancement of a direct absorption solar collector using copper oxide porous foam and nanofluid, Int. J. Energy Res. 44 (7) (2020) 5527–5544.

[17] S.P.A. Yegane, A. Kasaeian, Thermal performance assessment of a flat-plate solar collector considering porous media, hybrid nanofluid and magnetic field effects, J. Therm. Anal. Calorim. 141 (5) (2020) 1969–1980.

[18] N.F. Jouybari, T.S. Lundström, Performance improvement of a solar air heater by covering the absorber plate with a thin porous material, Energy 190 (2020) 116437.

[19] S. Saedodin, S. Zamzamian, M.E. Nimvari, S. Wongwises, H.J. Jouybari, Performance evaluation of a flat-plate solar collector filled with porous metal foam: experimental and numerical analysis, Energy Convers. Manag. 153 (2017) 278–287.

[20] S. Dhinakaran, J. Ponmozhi, Heat transfer from a permeable square cylinder to a flowing fluid, Energy Convers. Manag. 52 (5) (2011) 2170–2182.

[21] H.G. Weller, G. Tabor, H. Jasak, C. Fureby, A tensorial approach to computational continuum mechanics using object-oriented techniques, Comput. Phys. 12 (6) (1998) 620–631.

[22] F.P. Kärrholm, Numerical Modelling of Diesel Spray Injection, Turbulence Interaction and Combustion, Chalmers University of Technology Gothenburg, 2008.

[23] P. Roache, Perspective: a method for uniform reporting of grid refinement studies, J. Fluid Eng. 116 (3) (1994) 405–413.

[24] T. Morosuk, Entropy generation in conduits filled with porous medium totally and partially, Int. J. Heat Mass Tran. 48 (12) (2005) 2548–2560.

[25] A. Mohamad, Heat transfer enhancements in heat exchangers fitted with porous media Part I: constant wall temperature, Int. J. Therm. Sci. 42 (4) (2003) 385–395.

[26] K. Anirudh, S. Dhinakaran, On the onset of vortex shedding past a two-dimensional porous square cylinder, J. Wind Eng. Ind. Aerod. 179 (2018a) 200–214.

[27] K. Anirudh, S. Dhinakaran, Effects of Prandtl number on the forced convection heat transfer from a porous square cylinder, Int. J. Heat Mass Tran. 126 (2018b) 1358–1375.